Elastic buckling of thin-walled steel columns with periodic perforations

F.H. Smith[1], C.D. Moen[2]

Abstract
Finite strip eigen-buckling methods are introduced and validated through finite element eigen-buckling studies for calculating the local, distortional, flexural, and flexural-torsional elastic buckling of open thin-walled steel columns with periodic perforations. The goal in developing these simplified elastic buckling prediction methods is to provide an alternative to often cumbersome thin shell finite element modeling and, in research to come, the tools to accurately predict capacity of cold-formed steel rack sections, including the influence of holes, without the need for physical testing. For local buckling, an elastic plate buckling coefficient is derived with an energy solution considering hole size and frequency. The coefficient, which is lower to reflect the influence of holes on local buckling, is represented as a reduced cross-section element thickness in a finite strip analysis. For distortional buckling, the reduction in transverse web bending stiffness bracing the compression flanges is found to be a function of the planar net and gross areas of the perforated web element and is used to the modify web thickness in a finite strip analysis. For global buckling two viable methods are proposed for calculating the elastic buckling load including hole patterns. The first is a weighted average approach employing the classical cubic buckling equation and the second is simply to multiply the buckling load of the unperforated member by a ratio of the weighted average to gross-section properties of moment of inertia for flexural buckling and the St. Venant torsion constant for flexural-torsional buckling.

1. Introduction
This paper presents and validates approximate methods for characterizing the elastic buckling behavior of thin-walled steel columns with periodic perforation patterns typical of cold-formed steel rack columns. The elastic buckling solution methods are also potentially applicable to hot-rolled steel columns with periodic perforations, slit steel thermal studs, acoustic cold-formed steel metal decks, and cellular structures in the aerospace industry.

Steel pallet rack columns are punched with hole patterns along their length to accommodate rack shelf connections as shown in Fig. 1. The influence of these perforations on column compressive strength is treated in the U.S. with the Rack Manufacturers Institute's (RMI) Q factor method (RMI 2008) and in Europe with the European Committee for Standardization's (CEN) modification to the effective width method (CEN 2009). Both the Q factor method and the

---

[1] Graduate Research Assistant, Virginia Tech, <fhsmith@vt.edu>
[2] Assistant Professor, Virginia Tech, <cmoen@vt.edu>

modified effective width method rely on stub column tests to characterize the reduction in local buckling strength from perforations. In the RMI design approach, the Q factor ignores the influence of holes on distortional and global buckling capacities, both of which have been shown to decrease with the presence of holes (Hancock 1984; Moen and Schafer 2009a; Sarawit 2003). For these reasons, the RMI has begun exploring a more general, equation-based alternative to strength prediction through the efforts of researchers in the U.S. and Europe (e.g., Casafont et al. 2012), with a focus on the Direct Strength Method. This research was conducted in support of these efforts.

Figure 1: Storage rack a) assembly and b) shelf connection (UNARCO 2012)

The current state-of-the art in open thin-walled steel column design is the Direct Strength Method (DSM) (AISI 2007; Schafer 2008). A designer using the DSM will determine the critical elastic buckling loads for local ($P_{cr\ell}$), distortional (P_{crd}), and global or Euler buckling (P_{cre}) with finite strip eigen-buckling analysis of the column cross-section. These elastic buckling parameters are used to calculate slenderness values that are input into design equations to predict column capacity.

Perforations affect behavior of open thin-walled steel cross-sections and thus affect local, distortional, and global critical elastic buckling loads. Axial and bending stiffness of perforated elements (e.g., web and flange) is reduced, which can amplify local buckling deformation and decrease post-buckling capacity (Yu and Davis 1973). Cross-section deformation from distortional buckling is also amplified because the presence of web holes decreases the stabilizing influence of the web on the section (Hancock 1984; Moen and Schafer 2009a; Moen et al. 2013). Perforation patterns reduce global stiffness and capacity of the cross-section (Sarawit 2003) but reduction of these values is typically less severe than local or distortional buckling.

The DSM now addresses observed effects of discrete perforations in cold-formed steel columns and beams, for example a C-section wall stud with punched holes at 24 in. on center. The critical elastic buckling loads ($P_{cr\ell}$, P_{crd}, P_{cre}) are calculated *including the influence of holes* with

approximate classical plate and column buckling hand solutions and extensions to traditional finite strip analysis (Moen and Schafer 2009a; Moen and Schafer 2009b). The presence of holes typically reduces $P_{cr\ell}$, P_{crd}, and P_{cre}, causing cross-sectional and global slenderness to increase, for example $\lambda_c = (P_y/P_{cre})^{0.5}$, which results in a decrease in predicted capacity. The DSM equations also address the possibility of inelastic buckling and yielding of the net cross section at a hole by limiting the column capacity to $P_{ynet} = A_{net}F_y$. A final check of the three limit states results in the column capacity including the influence of holes, i.e., $P_n = \min(P_{ne}, P_{n\ell}, P_{nd})$.

Periodic perforations differ from discrete perforations in that they are smaller in size, are more tightly spaced, may contain more than one row of holes across the web or flanges of a cross-section, and are arranged in a pattern over the length of the member. Past research on the topic of columns with periodic perforations is of wide variety and has only recently considered the DSM (Casafont et al. 2012). An investigation of elastic buckling and strength of local and distortional modes for thermal studs was performed by Kesti (2000). Sarawit (2003) examined elastic local and global buckling and strength of three different rack sections. A method that forgoes elastic buckling prediction to find column strength and considers two different rack sections was lead by Davies (Davies et al. 1998). Pu and a team of researchers investigated the effect of multiple perforations in hot-rolled and cold-formed steel stub columns (Pu et al. 1999). Channel stub columns that featured circular (Rhodes and Schneider 1994) and slotted (Rhodes and Macdonald 1996) perforations were also tested. Hancock researched the effect perforations have on elastic distortional buckling and distortional buckling strength of three rack sections (Hancock 1984).

This paper investigates new finite strip approaches for calculating $P_{cr\ell}$, P_{crd}, and P_{cre} including the influence of periodic perforations. The methods are validated with thin-shell finite element eigen-buckling models of common rack cross-sections featuring web perforation patterns and recommendations are presented in a format consistent with the American Iron and Steel Institute's (AISI) North American Specification for the Design of Cold-Formed Steel Structural Members. The elastic buckling prediction results are compared to methods developed at the Polytechnic University of Catalonia (Casafont et al. 2012), to be known as Catalan prediction methods herein.

2. Thin Shell Finite Element Eigen-Buckling Parametric Studies
Seven perforation parameters were identified to potentially affect elastic local, distortional, and global buckling for rack sections: longitudinal perforation dimension, longitudinal perforation pitch, transverse perforation dimension, transverse perforation pitch, member shape, member thickness, and member length. A series of ABAQUS eigen-buckling analyses were conducted to examine the effect of these parameters on elastic buckling. The boundary and loading conditions of the models used in the analyses are shown in Fig. 2.

Cross-section shapes in this study (Fig. 3 and Table 1) were chosen to be similar to rack members in previous research (Casafont et al. 2012; Sarawit 2003). Base metal thicknesses used in this research were 1.8 mm, 2.0 mm, 2.5 mm. Fig. 4 and Table 2 show perforation dimensions and nomenclature. Perforation edge spacing in the transverse and longitudinal directions (s_{le} and s_{te}) was selected to be half of the perforation pitch (s_l and s_t). The number of holes in a local buckling half-wave is equal to $L_{cr\ell}/s_l$ for the longitudinal direction and n_t for the transverse, where $L_{cr\ell}$ is the local buckling half-wavelength. Two column lengths were considered –

$2.5L_{crd,nh}$ and $4L_{crd,nh}$ rounded up to the nearest $2h_o$ for modeling purposes, where $L_{crd,nh}$ is the cross-section distortional buckling half-wavelength, calculated in the finite strip software CUFSM (Li and Schafer 2010) neglecting the influence of holes. These physical lengths were selected because they can accommodate local, distortional, and global buckling deformations expected in rack members. Models were separated into two data sets: one featuring models with a set pitch and two transverse rows of web perforations typical of rack sections, another featuring varied pitch and row parameters.
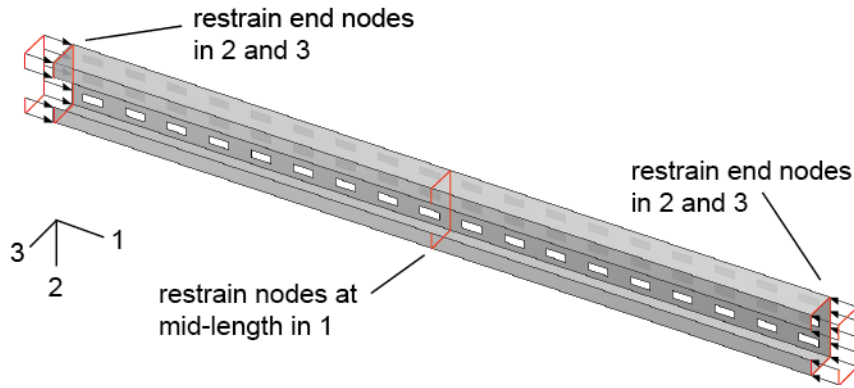
Figure 2: Finite element model boundary and loading conditions

To reduce the amount of variables tested, four two-letter perforation combinations were assigned to each permutation of member shape and length (Table 3). Each letter combination considered n_t and $L_{cr\ell}/s_l$ values in Table 2 associated with the letter combination's perforation dimensions. For example, one of the four perforation combinations assigned to models where shape = 3, L = $2.5L_{crd}$, and t = 1.8 mm was "CE". The "CE" combination represents hole patterns where L_h = "C" and d_h = "E", i.e., $L_h = 0.25h_o$ and $d_h = 0.125h_o$. This case tests patterns with the following numbers of holes:

1. $L_{cr\ell}/s_l = 1$ → $n_t = 1, 2, 3$
2. $L_{cr\ell}/s_l = 1.5$ → $n_t = 1, 2, 3$
3. $L_{cr\ell}/s_l = 2$ → $n_t = 1, 2, 3$

or 9 permutations. The "CE" combination also represents the case where L_h = "E" and d_h = "C", i.e., $L_h = 0.125h_o$ and $d_h = 0.25h_o$. These hole dimensions test the following numbers of holes:

1. $L_{cr\ell}/s_l = 1$ → $n_t = 1, 2$
2. $L_{cr\ell}/s_l = 1.5$ → $n_t = 1, 2$
3. $L_{cr\ell}/s_l = 2$ → $n_t = 1, 2$
4. $L_{cr\ell}/s_l = 3$ → $n_t = 1, 2$

or 8 permutations. So for the letter combination "CE", a total of 17 different models were tested.

Table 1: Shape Dimensions

Shape	h_o (mm)	b_o (mm)	D (mm)	θ (deg)	b_2 (mm)	D_2 (mm)
1	72	36	18	-	-	-
2	72	72	18	-	-	-
3	72	36	13.4	63.4	30	12
4	72	90	21.2	45	39	15
5	108	30	17.5	59.0	33	15
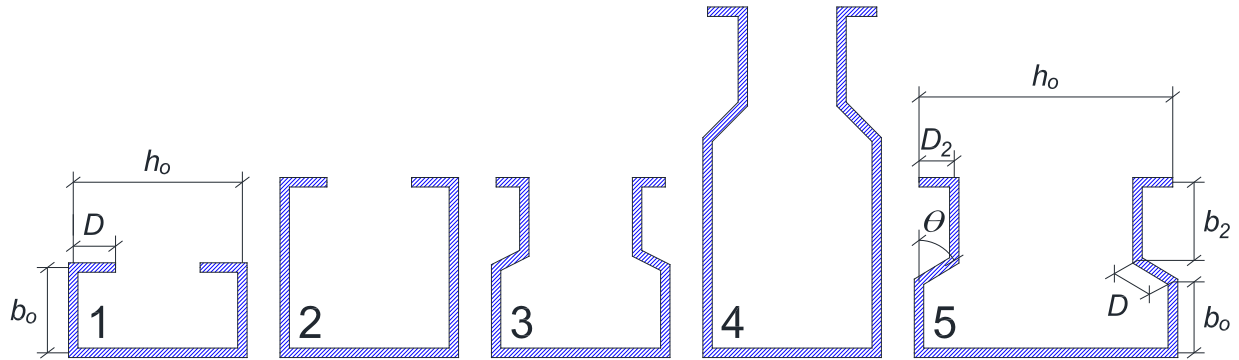
Figure 3: Shapes

Table 2: Perforation Schedule

Hole Dimension (L_h or d_h)/h_o	Dimension Name	Rack Data Set		Full Data Set	
		$L_{cr\ell}/s_l$	n_t	$L_{cr\ell}/s_l$	n_t
0.375	A	1.5	-	1, 1.5	1
0.313	B	1.5	-	1, 1.5	1
0.250	C	1.5	-	1, 1.5, 2	1, 2
0.188	D	-	2	1, 1.5, 2	1, 2
0.125	E	-	2	1, 1.5, 2, 3	1, 2, 3
0.094	F	-	2	1, 1.5, 2, 3	1, 2, 3
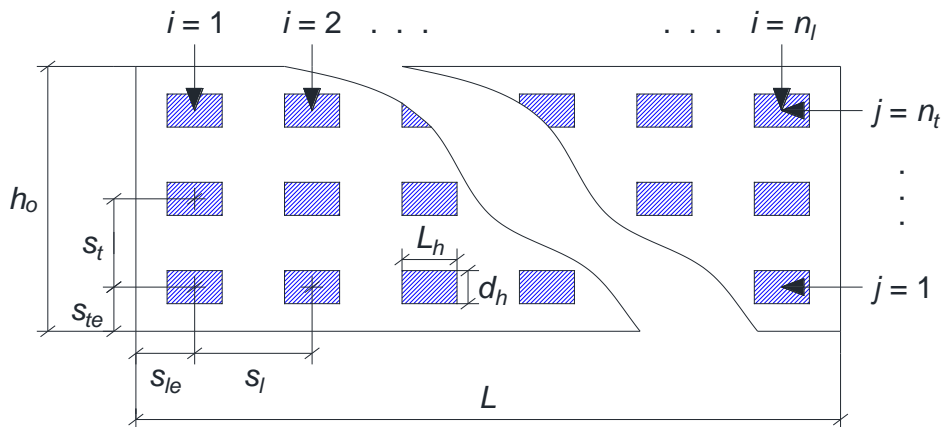
Figure 4: Column Perforation Nomenclature

Table 3: Column Schedule

t (mm)	L/L_{crd}	Shape 1	2	3	4	5
1.8	2.5	FF	AA	DD	CC	EE
		AB	AC	AD	AE	AF
		CD	BE	BF	BD	BC
		EF	DF	CE	CF	DE
	4	DD	FF	CC	EE	BB
		AF	AB	AC	AD	AE
		BD	CF	BE	BC	CD
		CE	DE	DF	EF	BF
2	2.5	AA	CC	EE	BB	FF
		AC	AD	AE	AF	AB
		BF	BC	BD	BE	CE
		DE	EF	CF	CD	DF
	4	EE	DD	BB	AA	CC
		AE	AF	AB	AC	AD
		BC	BD	CD	BF	BE
		DF	CE	EF	DE	CF
2.5	2.5	BB	EE	AA	FF	DD
		AD	AE	AF	AB	AC
		BE	BF	BC	CE	BD
		CF	CD	DE	DF	EF
	4	CC	BB	FF	DD	AA
		AC	AB	AD	AF	AE
		BF	CD	BE	BD	BC
		DE	EF	CF	CE	DF

Buckling modes of the finite element models were visually identified by finding the buckled half-wave with the greatest magnitude (using color topography featured in Fig. 5a and 5b) and classifying the mode based on that deformation's length and shape. This method allowed for the distinction to be made when local and distortional buckling mixed (Fig. 5a and 5b), and for other mixed mode cases. The lowest modes that exhibited local, symmetric distortional, asymmetric distortional, flexural, and flexural-torsional buckling were recorded.

The influence of perforation patterns on elastic buckling for the models studied can be found in Table 3; note that the subscripts h and nh denote perforated and unperforated models. For most cases the presence of holes decreased the buckling loads. The increase in the critical elastic local buckling load (max of 1.25 in Table 3) was caused because perforations can sometimes change the quantity and length of the local half-waves (Moen and Schafer 2009b).

Table 3: Effect perforations have on finite element results (1282 models)

Mode	Flexural Buckling	Flexural-Torsional Buckling	Distortional Buckling	Local Buckling
	$(P_{cre,f,h}/P_{cre,f,nh})_{ABAQUS}$	$(P_{cre,ft,h}/P_{cre,ft,nh})_{ABAQUS}$	$(P_{crd,h}/P_{crd,nh})_{ABAQUS}$	$(P_{cr\ell,h}/P_{cr\ell,nh})_{ABAQUS}$
Min	0.72	0.83	0.63	0.48
Max	0.99	1.00	1.04	1.25
Mean	0.92	0.97	0.95	0.91
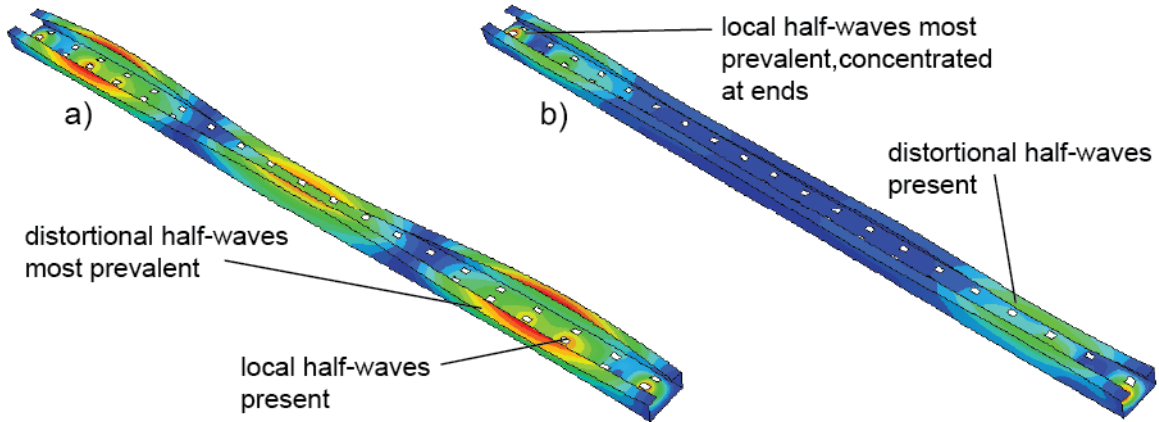
Figure 5: Elastic buckling modes: (a) distortional buckling, (b) local buckling

Critical local buckling modes typically featured half-wave deformations with the greatest magnitudes concentrated at both ends of the column (Fig. 5b). Symmetric distortional buckling was prone to mixing with local buckling, as shown in Fig. 5a, and perforations caused half-wavelengths to vary in length. Pertaining to asymmetric distortional buckling (Fig. 6a and 6b), several observations were made. Double curvature of the web forced local buckling deformations to the flanges in asymmetric distortional mode mixing and because most models featured flange stiffeners; the five models featuring mode mixing were limited to shape 2 which did not feature flange stiffeners. Asymmetric distortional buckling never governed for shape 1 as the stiffness of the web in double curvature was increased due to the shape's small flange to web ratio. Asymmetric distortional buckling governed more often in longer members – compare 380 cases where $L = 4L_{crd,nh}$ to 1 case where $L = 2.5L_{crd,nh}$. It is believed that the longer half-wavelengths of asymmetric compared to symmetric distortional buckling combined with the finite length of the models contributed to member length influencing which mode governed. Flexural-torsional buckling governed global buckling for all models and never featured mode mixing as $P_{cre,ft}$ was always much lower than $P_{cr\ell}$ and P_{crd}. Flexural buckling had a tendency to mix modes with distortional buckling – this was identified by flanges bending outward as the shape buckled in the weak axis direction. Fig. 6b and 6c show flexural-torsional and mixed flexural and distortional buckling mode shapes.

Finite strip elastic buckling methods are introduced in the following sections that attempt to reflect the behavior observed in the finite element analyses while being simple and accessible to designers.
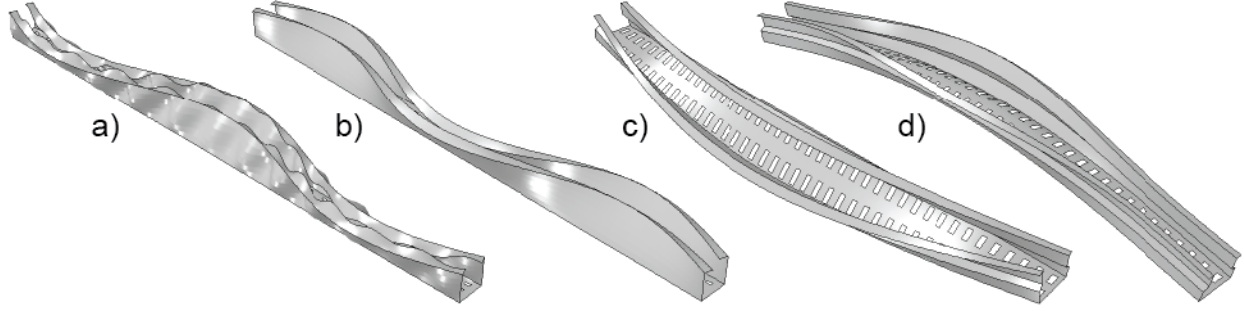
Figure 6: Models exhibiting a) local-asymmetric-distortional buckling interaction, b) asymmetric-distortional buckling, c) flexural-torsional buckling, and d) flexural-symmetric-distortional buckling interaction

3. Global Buckling of Thin-Walled Steel Columns with Periodic Perforations

3.1 Flexural Buckling

The critical elastic flexural buckling load including the influence of periodic perforations, $P_{cre,f,h}$, is approximated as

$$P_{cre,f,h} = P_{cre,f,nh} \frac{I_{avg}}{I_g} \tag{1}$$

where

$$I_{avg} = \frac{I_g L_g + I_{net} L_{net}}{L}. \tag{2}$$

The Euler buckling load without perforations, calculated with classical equations or finite strip analysis, is $P_{cre,f,nh}$ and I_{net} and I_g are the net and gross cross-section moment of inertia about the weak or strong axis. In the cases studied herein, $L_{net} = n_l L_h$ is the total length of net section along the column and $L_g = L - L_{net}$.

3.2 Flexural-Torsional Buckling

The critical elastic buckling load for flexural-torsional buckling, $P_{cre,ft,h}$, including the influence of periodic perforations is approximated as

$$P_{cre,ft,h} = \frac{A_g}{2\beta_h}\left[\left(\sigma_{ex,h} + \sigma_{t,h}\right) - \sqrt{\left(\sigma_{ex,h} + \sigma_{t,h}\right)^2 - 4\beta_h \sigma_{ex,h}\sigma_{t,h}} \right] \tag{3}$$

where

$$\beta_h = 1 - \left(\frac{x_{o,avg}}{r_{o,avg}}\right)^2 \tag{4}$$

283

$$\sigma_{ex,h} = \frac{\pi^2 E I_{x,avg}}{A_g (K_x L_x)^2} \tag{5}$$

$$\sigma_{t,h} = \frac{1}{A_g r_{o,avg}^2} \left[G J_{avg} + \frac{\pi^2 E C_{w,net}}{(K_t L_t)^2} \right]. \tag{6}$$

The elastic modulus is E, the shear modulus is G, and KL, $K_x L_x$, and $K_t L_t$ are the effective column lengths about the axis of bending, the x centroidal axis, and torsional axis respectively. The x distance from the centroid to the shear center for the weighted cross-section is $x_{o,avg}$. The weighted average radius of gyration about the shear center is calculated using $r_{o,avg} = (r_{x,avg}^2 + r_{y,avg}^2 + x_{o,avg}^2)^{0.5}$ where $r_{x,avg}$ and $r_{y,avg}$ are the weighted average radii of gyration about the centroidal axes calculated using $r_{x,avg} = (I_{x,avg}/A_{avg})^{0.5}$ and $r_{y,avg} = (I_{y,avg}/A_{avg})^{0.5}$. The weighted average moment of inertia about the centroidal axes are $I_{x,avg}$ and $I_{y,avg}$ and A_{avg} is the weighted average area of the cross-section. The weighted average area A_{avg} should not be substituted for the gross cross-section area A_g in the denominator because A_g accounts for the conversion of stress to force at member ends. The warping torsion constant at the net section is $C_{w,net}$. This net section property (as well as the net section properties needed to calculate $x_{o,avg}$, $I_{x,avg}$, $I_{y,avg}$, A_{avg}, and J_{avg}) can be determined with the section property calculator in CUFSM by setting the element thickness to zero at the hole locations in the cross-section. All weighted average properties are calculated in the same manner as Eq. 2.

The above approach can be cumbersome, and therefore an alternative approach for calculating $P_{cre,f,h}$ is proposed that can be directly applied with finite strip analysis

$$P_{cre,ft,h} = P_{cre,ft,nh} \frac{J_{avg}}{J_g} \tag{7}$$

where $P_{cre,ft,nh}$ is the critical elastic flexural-torsional buckling load of the unperforated shape that can be calculated using finite strip analysis, J_{net} and J_g are the net and gross section St. Venant torsion constants, and J_{avg} is the weighted average St. Venant torsion constant calculated in the same manner as Eq. 2. Accuracy of the proposed methods is evaluated in the following section.

3.3 Validation
Flexural and flexural-torsional buckling prediction results using Eq. 1 (classical and finite strip solutions), Eq. 3, Eq. 7 and the Catalan method are compared in Table 5. The comparisons are presented both for the models that most represented typical rack perforations and for all the models considered. The more complicated classical weighted average approach in Eq. 1 and 3 and the simple version in Eq. 1 and 7 (using CUFSM for both) are all accurate predictors of flexural and flexural-torsional buckling loads. The Casafont et al. (2012) method is accurate for flexural-torsional buckling however the COV is high for flexural buckling. This can be explained by the method being prone to exhibit distortional buckling at half-wavelengths equal to member length and the batch program used to retrieve results was not sophisticated enough to determine all cases where this occurred. Visually investigating higher buckling modes may improve the Catalan method's accuracy.

Table 5: ABAQUS to predicted statistics for global buckling

Mode	Flexural Buckling[1]				Flexural-Torsional Buckling			
Data Set	Rack Sections		All Sections		Rack Sections		All Sections	
No. of Models	47		1155		54		1282	
Method	Mean	COV	Mean	COV	Mean	COV	Mean	COV
Eq. 1 and 7 (CUFSM)	**0.95**	**0.03**	**0.96**	**0.04**	**0.98**	**0.01**	**0.99**	**0.02**
Eq. 1 and 3 (Classical)	0.91	0.07	0.92	0.06	0.99	0.02	1.00	0.05
Casafont et al. 2012	0.95	0.13	0.99	0.11	1.06	0.03	1.06	0.04

1. Finite element eigen-buckling analyses did not exhibit flexural buckling within first 150 modes calculated for Shape 4 models where $L = 2.5L_{crd,nh}$.

4. Distortional Buckling of Thin-Walled Steel Columns with Periodic Perforations

4.1 Prediction Method
The critical elastic distortional buckling load including the influence of web periodic perforations, $P_{crd,h}$, is approximated in a finite strip analysis by reducing the thickness of the cross-section web to

$$t_{r,d} = t\left(1 - \frac{n_l n_t L_h d_h}{L h_o}\right)^{\frac{1}{3}}.$$

(8)

A finite strip reference stress is applied to the modified cross-section and $P_{crd,h}$ is taken as the minimum buckling load on the distortional buckling branch of the elastic buckling curve.

4.2 Supporting Derivation
The method proposed in Section 4.1 is a variation of that developed by Moen and Schafer (2009a). A simply-supported web plate equal in length to the distortional half-wavelength of the unperforated cross-section is modeled with an imposed rotation along the longitudinal edges of the plate that varied in magnitude proportional to a half sine wave, mimicking the behavior of the web in distortional buckling. Moments at the longitudinal edges of the plates corresponding to the imposed deflection were recorded to determine rotational stiffness of the web plate. Fig. 7 shows the loading and boundary conditions of the web rotational restraint study.
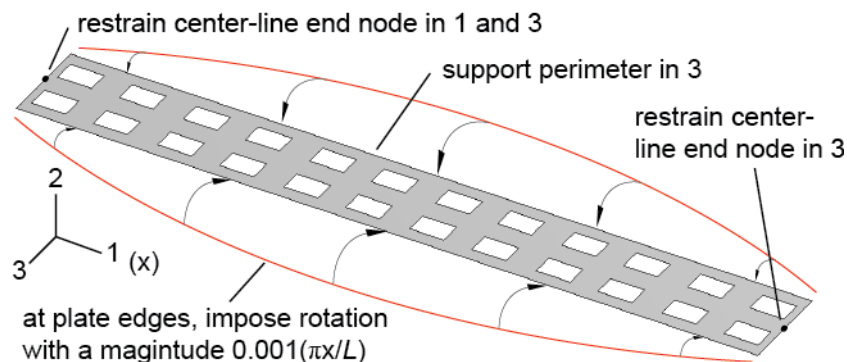
Figure 7: Web rotational restraint loading and boundary conditions

If $K_{\theta,h}$ and $K_{\theta,nh}$ are assumed to be the average cumulative transverse rotational stiffness of plates with and without perforations, an equation describing the reduced thickness of the web plate can be developed. This equation was derived by Moen and Schafer (2009a) as

$$t_r = t\left(\frac{K_{\theta,h}}{K_{\theta,nh}}\right)^{\frac{1}{3}} . \tag{9}$$

Based on the results from the finite element model in Fig. 8, it is concluded that the reduction in transverse web bending stiffness within a distortional buckling half-wave can be represented using the ratio of the web's planar net area ($n_l n_t L_h d_h$) to the web's planar gross area along the column (Lh_o)

$$K_{\theta,h} = \left(1 - \frac{n_l n_t L_h d_h}{Lh_o}\right)K_{\theta,nh} . \tag{10}$$
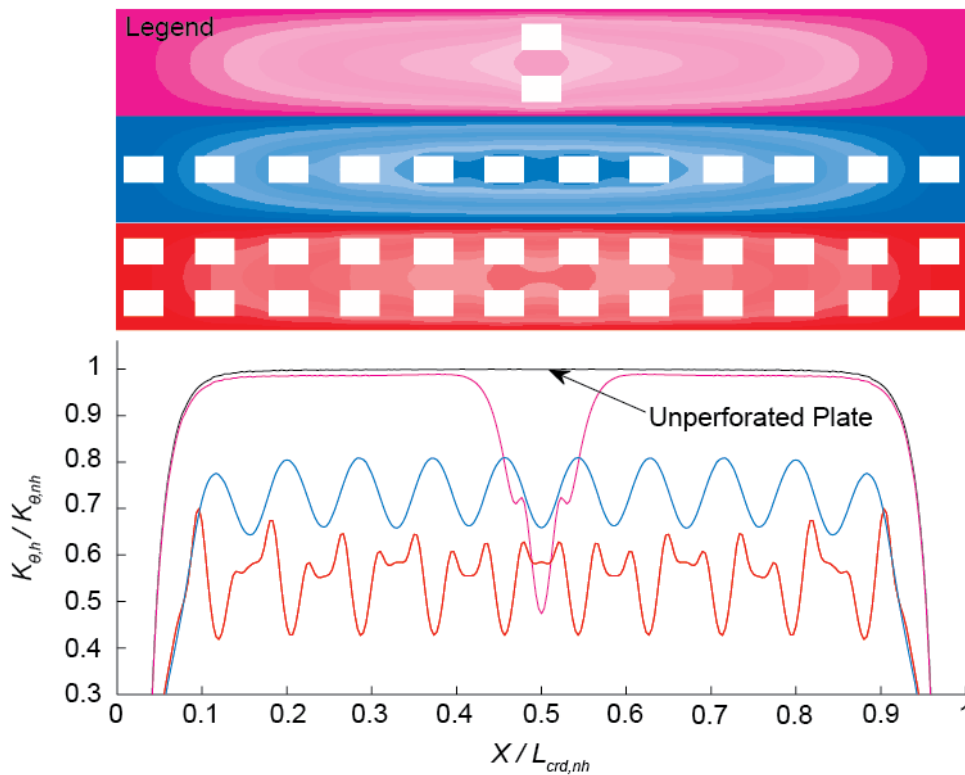
Figure 8: Transverse rotational stiffness of web plates with periodic perforations

Although the distortional buckling half-wavelength is not required to calculate $P_{crd,h}$ it is still interesting to mention that L_{crd} typically increased with the presence of perforation patterns. As web rotational stiffness decreased, half-wavelength generally increased and of the contributing factors, perforation length had the greatest contribution.

286

4.3 Validation

Prediction accuracy for the finite strip distortional buckling method is presented in Table 6. Accuracy of the method proposed in Section 4.1, i.e., reducing the web thickness using Eq. 8 in a finite strip analysis, is consistent with the approach in Casafont et al. (2012). This is not surprising since both approaches are founded on the same idea that web perforations reduce transverse bending stiffness.

Table 6: ABAQUS to predicted statistics for distortional buckling

Data Set	Rack Sections		All Sections	
No. of Models	54		1282	
Method	Mean	COV	Mean	COV
Eq. 8	**0.97**	**0.08**	**1.02**	**0.09**
Casafont et al. 2012	1.11	0.09	1.13	0.10

5. Local Buckling of Thin-Walled Steel Columns with Periodic Perforations

5.1 Prediction Method

The critical elastic local buckling load including the influence of periodic perforations, $P_{cr\ell,h}$, is approximated in a finite strip analysis by reducing the thickness of each stiffened element in a cross-section containing perforations to

$$t_{r,\ell} = t\left[1 - \frac{n_l n_t\left(L_h d_h - \mu L_h \beta Y^* - \mu d_h \alpha X^* + \alpha X^* \beta Y^*\right)}{Lh_o}\right]^{\frac{1}{2}} \tag{11}$$

where μ is Poisson's ratio, longitudinal and transverse hole shape factors are α and β, and the longitudinal and transverse hole location factors are X^* and Y^*.

$$\alpha = \frac{h_o}{\pi}\sin\left(\frac{\pi L_h}{h_o}\right) \tag{12}$$

$$\beta = \frac{h_o}{\pi}\sin\left(\frac{\pi d_h}{h_o}\right) \tag{13}$$

$$X^* = -0.5 \tag{14}$$

$$Y^* = \begin{cases} 0 & if \quad n_t = 1 \\ -1 & if \quad n_t \neq 1 \end{cases} \tag{15}$$

A finite strip reference stress is applied to the modified cross-section and $P_{cr\ell,h}$ is taken as the minimum buckling load on the local buckling branch of the elastic buckling curve.

5.2 Supporting Derivation

The reduced thickness in Eq. 11 was derived using a plate buckling coefficient including the influence of perforations. A Rayleigh-Ritz energy solution was employed where equilibrium in the deformed state considers the strain energy of the plate at the perforations to be absent. This can be shown as

$$\delta(U_{nh} - U_h + W) = 0 \tag{16}$$

where U_{nh} is the strain energy of the deformed plate, U_h is the total strain energy at the location of the perforations, and W is the external work applied to the plate by a uniform traction load, N_{cr}. The strain energy equations compute the strain energy of the deformed plate using an approximation of the buckled shape, shown in Eq. 17 (Chajes 1974). The assumed deformation considers a simply supported plate able to deform in multiple half sine waves in the longitudinal, x, and transverse, y, directions.

$$w = \sum_{m=1}^{\infty} \sum_{n=1}^{\infty} A_{m,n} \sin\frac{m\pi x}{L} \sin\frac{n\pi y}{h_o} \tag{17}$$

In Eq. 17, m is the number of half sine waves in the longitudinal direction, n is the number of half sine waves in the transverse direction and A is an array of arbitrary constants that define the magnitude of displacement for each combination of m and n. This equation does not consider the influence of holes on the shape and size of buckling deformations.

Solving for the critical elastic traction load, N_{cr}, is done in a similar manner taken by Chajes (1974). This approach yields

$$N_{cr} = \frac{\pi^2 E t^3}{12(1 - \mu^2)h_o^2} k_h. \tag{18}$$

The plate buckling coefficient considering perforations, k_h, has been simplified by the following assumptions:

1. Longitudinal perforation spacing is equal to the length of the web plate divided by the number of longitudinal holes, i.e., $s_l = L/n_l$.
2. Transverse perforation spacing is equal to the width of the web plate divided by the number of transverse holes, i.e., $s_t = h_o/n_t$.
3. The perforated pattern is aligned symmetrically on the web plate. In conjunction with assumptions 1 and 2, this gives us edge spacings equal to half their respective pitch, i.e., $s_{le} = s_l/2$ and $s_{te} = s_t/2$.
4. The ratio of web plate length to width (L/h_o) is a positive integer.
5. Perforations do not affect the number of longitudinal and transverse half waves that correlate to the minimum value of k_{nh}, i.e. $m = L/h_o$ and $n = 1$.

For long perforated plates, assumptions 1, 3, and 4 are good approximations for all cases and are met by our models. Without assumption 5, k_h considers the effect of perforations on the critical

number of half-waves (though not the shape of the half-waves); however, in doing so, one needs to iterate to determine the minimum value of k_h. Assumption 5 is seen as a practical approximation, as it allows for k_h to be solved directly. This is justified because differences between considering and not considering assumption 5 were infrequent (28 out of 1282 times) and had minimal effect when they did occur (the minimum value of $k_{h,min}/k_{h,assumption}$ was 0.926). The resulting simplification of k_h becomes

$$k_h = 4\left[1 - \frac{n_l n_t \left(L_h d_h - \mu L_h \beta Y - \mu d_h \alpha X + \alpha X \beta Y\right)}{Lh_o}\right] \tag{19}$$

where α and β (Eq. 12 and 13) are constants related to the size of perforations relative to the size of the assumed buckling deformations and X and Y (Eq. 20 and 21) are step functions that account for the perforation pattern position relative to buckled half waves. Represented by multiplying $n_l n_t X$ or $n_l n_t Y$ is the cumulative sum of the effect that each perforation has on strain energy due to that perforation's location within a buckling deformation in the longitudinal or transverse direction. For example, if X equals zero, then a case is described where the position effect of each hole in the longitudinal direction, when taken collectively, is $n_l n_t(0)$, or net zero. If X is equal to negative one, holes are only aligned in a position that removes the most strain energy from the system, i.e., on the points of maximum deflection. If X is equal to positive one, holes remove the least strain energy from the system and thus are positioned on the points with zero deflection. The same logic can be applied to Y in the transverse direction.

$$X = \begin{cases} -1 & if & \dfrac{n_l h_o}{L} = \frac{1}{1}, \frac{1}{3}, \frac{1}{5}, \cdots \\[2mm] 1 & if & \dfrac{n_l h_o}{L} = \frac{1}{2}, \frac{1}{4}, \frac{1}{6}, \cdots \\[2mm] 0 & if & \dfrac{n_l h_o}{L} \neq \frac{1}{1}, \frac{1}{2}, \frac{1}{3}, \cdots \end{cases} \tag{20}$$

$$Y = \begin{cases} -1 & if & n_t = 1 \\ 0 & if & n_t \neq 1 \end{cases} \tag{21}$$

An equation for the reduced thickness of the web plate (Eq. 22) can be derived by comparing equations for the critical buckling stress of a plate considering perforations.

$$\sigma_{cr,h} = \frac{\pi^2 E t^2}{12(1-\mu^2)h_o^2} k_h = \frac{\pi^2 E t_{r,l}^2}{12(1-\mu^2)h_o^2} k_{nh} \rightarrow t_{r,l} = t\left(\frac{k_h}{k_{nh}}\right)^{\frac{1}{2}} \tag{22}$$

When substituting the hole location factors, X and Y, into Eq. 19 and assuming the plate to be long, i.e., $k_{nh} = 4$, Eq. 22 simplifies to become similar to the recommended reduced thickness in Eq. 14. ABAQUS to predicted means from this method (0.84 for rack models and 0.96 for all models)reveal a fundamental difference in buckling behavior between rack sections and all sections tested that is not accounted for – the number of holes per longitudinal and transverse

half-waves affects local buckling capacity. Addressing this can be done in one of two ways: either by determining a new deformation function, w, which considers holes' effect on displaced shape or by adjusting X and Y, which can be seen as an approximation of a new deformation function. The latter was done in an effort to forgo additional complexity.

The first step taken to modify X and Y was examining extreme cases of local buckling to gather insight into how deformations may affect longitudinal and transverse behavior of local buckling. Though the assumption was made that buckled half-waves are equal in length and width, this is not always the case as shown in Fig. 9. These extrema show the number of transverse half-waves, n, will always equal the assumption of one, but they also show the assumption that the number of longitudinal half-waves, m, is equal to L/h_o to be incorrect. It is hypothesized that for long plates, a single optimum cumulative strain energy effect in the longitudinal direction will be reached by m, regardless of perforation pattern, if m is allowed to step toward the lowest energy solution. This is analogous to X having one possible coefficient as it represents the effects of holes in regards to m and thus represents the lowest energy solution. Iteration to find the lowest value of k_h is eliminated by this assumption. Because rack sections are cases where $n_l h_o/L = 1.5$ and because these sections were predicted so poorly by the method using X and Y, the new single coefficient for X should not equal zero. In addition, it is logical to assume holes should have a negative effect on strain energy, however, the likelihood of each hole aligning at a peak or valley of deformations is low as half-waves are allowed to buckle freely in the longitudinal direction. Thus it is expected the value of X should be between negative one and zero. For the transverse direction, since n will always equal one, the location of holes in relation to the buckled half-wave is more accurately known, allowing for multiple coefficients to be considered for Y. When examining Fig. 9, for cases where only one hole is located along the width of the web, there seems to be little effect on the shape of the transverse half-wave compared to the case without holes, thus Y should not have an effect on strain energy and in turn equal zero. Other cases in Fig. 9 show buckled half-waves to change in shape in the transverse direction, where levels of maximum strain energy are extended some distance over the width of the plate. This suggests that when previously, holes had a net zero effect, the cumulative strain energy lost will be positive, thus making a new Y somewhere between negative one and zero.
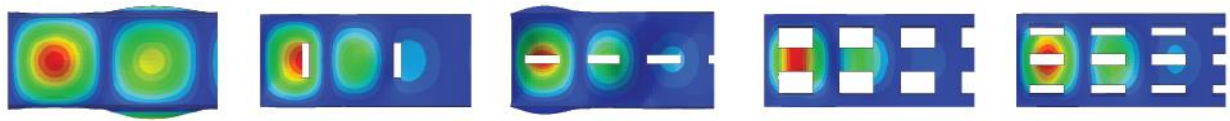
$P_{cr\ell,h,ABAQUS}/P_{cr\ell,nh,ABAQUS}$				
1.00	1.25	0.83	0.48	0.54
No. of Models				
30	2	4	3	2
Mean($P_{cr\ell,h,ABAQUS}$/Eq. 11)				
0.98	1.29	0.88	0.90	0.84

Figure 9: Local buckling extrema

The second step taken to modify X and Y was performing a graphical optimization to determine the modified factors X^* and Y^* (Eq. 14 and 15) considering observations in step one. Optimization (Fig. 10) confirmed the modified position factor in the transverse direction, Y^*, should be taken as zero when n_t was equal to one because for all cases of X^*, ABAQUS to predicted mean values were near unity. For other cases, optimization confirmed that the position

factor in the longitudinal direction should not equal to zero in order to minimize COV values. The values of -0.5 for X^* and -1.0 for Y^* were selected because these values minimized the COV values for cases where n_t was greater than one and provided accurate mean prediction for all cases.
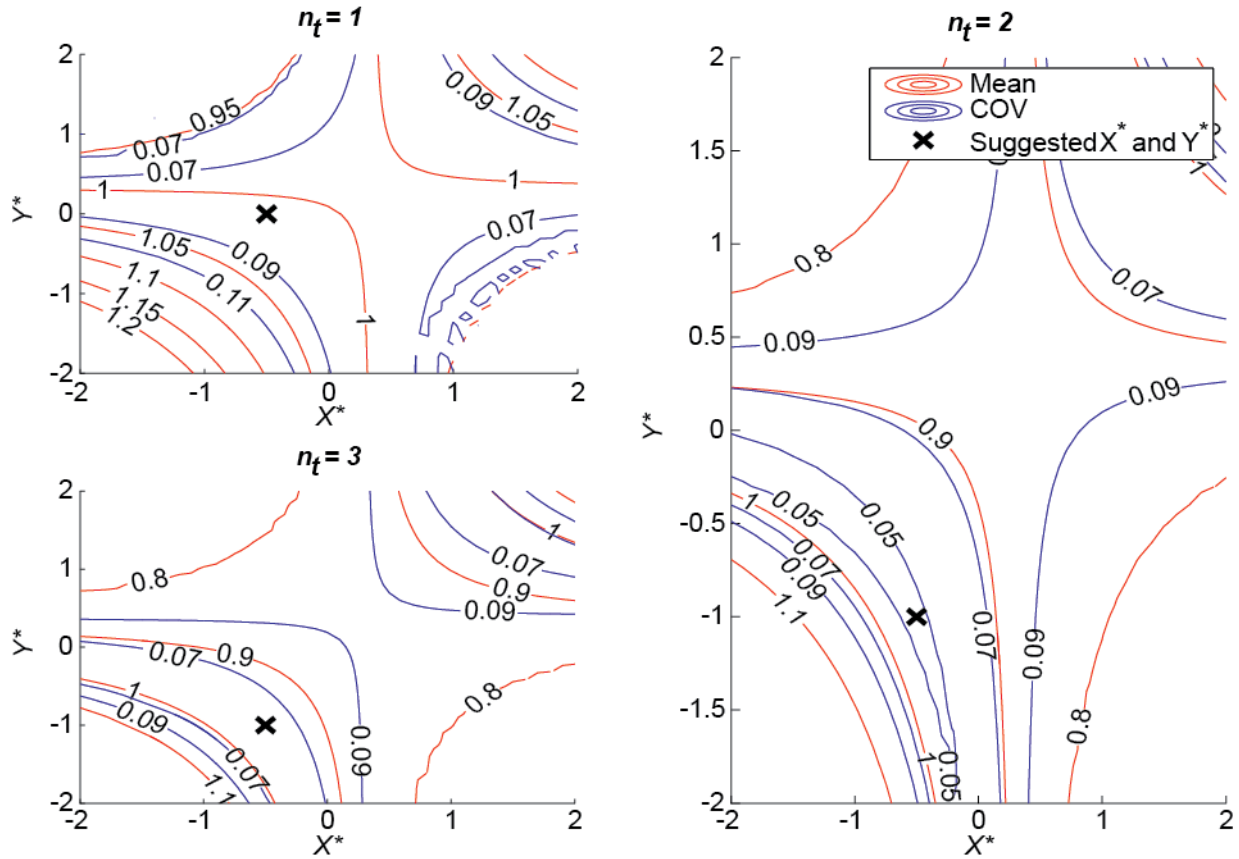
Figure 10: Graphical optimization of mean and COV, values in terms of ABAQUS to predicted

5.3 Validation

The finite strip local buckling method proposed in Section 5.1 is demonstrated to be an accurate predictor of critical elastic local buckling load including perforation patterns as shown in Table 7. The local buckling predictions are slightly unconservative on average, however the low COV compared to the Casafont et al. (2012) demonstrates the benefits of including plate buckling behavior in the prediction.

Table 7: ABAQUS to predicted statistics for local buckling

Data Set	Rack Sections		All Sections	
No. of Models	54		1282	
Method	Mean	COV	Mean	COV
Eq. 11	**0.92**	**0.05**	**0.97**	**0.08**
Casafont et al. 2012	0.86	0.14	0.80	0.22

6. Conclusions

Finite strip analysis methods for calculating the critical elastic global, distortional, and local buckling loads of thin-walled steel columns with periodic perforations are presented. The global buckling approach employs a ratio of the weighted average section properties to the gross section properties to reduce the Euler buckling load, and this same approach is extended to flexural-torsional buckling, providing a simple, general, and accurate finite strip approach to treating hole patterns. A reduced web thickness approach originally derived for discrete holes was extended to perforation patterns to include their influence on distortional buckling. Reducing the web thickness in a finite strip analysis simulates the loss of transverse stiffness bracing the compressed flanges from distortional buckling deformation. As the transverse stiffness decreases, i.e., as more hole area aggregates in the web, the distortional buckling half-wavelength increases. For local buckling, an energy solution of a perforated plate was employed to derive a reduced thickness equation that can be applied to any stiffened element in a cross-section containing perforation patterns. The cross-section is modified with these calculated reduced thicknesses, and then a finite strip analysis is performed to obtain the reduced local buckling load. The accuracy of the approximate methods were verified with a thin-shell finite element elastic buckling database of over 1200 models with varying cross-section, hole pattern, and hole size parameters. Research is ongoing to apply these new methods in the Direct Strength Method and compare strength predictions to test data.

References

American Iron and Steel Institute (AISI). (2007). *North-American Specification for the Design of Cold-Formed Steel Structural Members*. S100-07.

Casafont, M., Pastor, M., Bonada, J., Roure, F., Pekoz, T. (2012). "Linear buckling analysis of perforated steel storage rack columns with the Finite Strip Method." *Thin-Walled Structures*, Vol. 61, Dec. 2012, pp. 71-85.

Chajes, A. (1974). "Chapter 6 – Buckling of Plates." *Principles of Structural Stability Theory*, Prentice Hall, Englewood Cliffs, NJ., pp. 238-302.

Davies, J.M., Leach, P., Taylor, A. (1998). "The design of perforated cold-formed steel sections subject to axial load and bending." *Thin-Walled Structures*, Vol. 29, Nos. 1-4, pp. 141-157.

European Committee for Standardization (CEN). (2009). *Steel static storage systems – Adjustable pallet racking systems – Principles for structural design*. EN 15512:2009.

Hancock, G.J. (1984). "Distortional buckling of steel storage rack columns." *Proceedings of the Seventh International Specialty Conference on Cold-Formed Steel Structures*, St. Louis, MO., Nov. 13-14, 1984, pp. 345-373.

Kesti, J. (2000). *Local and distortional buckling of perforated steel wall studs*. Report TKK-TER-19. Laboratory of Steel Structures, Helsinki University of Technology.

Li, Z., Schafer, B.W. (2010) "Buckling analysis of cold-formed steel members with general boundary conditions using CUFSM: conventional and constrained finite strip methods." *Proceedings of the 20th International Specialty Conference on Cold-Formed Steel Structures*, St. Louis, MO., November, 2010.

Moen, C.D., Schafer, B.W. (2009a). "Elastic buckling of cold-formed steel columns and beams with holes." *Engineering Structures*, Vol. 31, No. 12, pp. 2812-2824.

Moen, C.D., Schafer, B.W. (2009b). "Elastic buckling of thin plates with holes in compression or bending." *Thin Walled Structures*, Vol. 47, No. 12, pp. 1597-1607.

Moen, C.D., Schudlich, A., von der Heyden, A. (2013). "Experiments on cold-formed steel joists with unstiffened web holes." *Journal of Structural Engineering* (to appear).

Pu, Y., Godley, M.H.R., Beale, R.G., Lau, H.H. (1999). "Prediction of Ultimate Capacity of Perforated Lipped Channels". *Journal of Structural Engineering*. ASCE, Vol. 125, No. 5, May 1999, pp. 510-514.

Rack Manufacturers Institute (RMI). (2008). *Specification for the Design, Testing and Utilization of Industrial Steel Storage Racks*. MH16.1-2008.

Rhodes, J., Schneider, F.D. (1994). "The Compressional Behaviour of Perforated Elements". *Proceedings of the Twelfth International Specialty Conference on Cold-Formed Steel Structures*, St. Louis, MO., Oct. 18-19, 1994, pp. 11-28.

Rhodes, J., Macdonald, M. (1996). "The Effects of Perforation Length on the Behaviour of Perforated Elements in Compression". *Proceedings of the Thirteenth International Specialty Conference on Cold-Formed Steel Structures*, St. Louis, MO. Oct. 17-18, 1996, pp. 91-101.

Sarawit, A.T. (2003). *Cold-formed steel frame and beam-column design*. Report 03-03. School of Civil and Environmental Engineering, Cornell University.

Schafer, B.W. (2008). "Review: the Direct Strength Method of cold-formed steel member design". *Journal of Constructional Steel Research*. Vol. 64, Nos. 7-8, 2008, pp. 776-778.

UNARCO Pallet Rack & Warehouse Storage Systems. (2012). *Pallet Rack Photo Gallery*. <www.unarcorack.com/> (Jan. 15, 2012).

Yu, W.W., Davis, C.S. (1973). "Cold-Formed Steel Members with Perforated Elements". *Journal of the Structural Division*. ASCE, Vol. 99, No. ST10, Oct. 1973, pp. 2061-2077.